Imaging guided trials of the angiogenesis inhibitor sunitinib in mouse models predict efficacy in pancreatic neuroendocrine but not ductal carcinoma

Peter Olson[a], Gerald C. Chu[b,c], Samuel R. Perry[b], Olivier Nolan-Stevaux[a], and Douglas Hanahan[a,1,2]

[a]Diabetes Center and Helen Diller Family Comprehensive Cancer Center, University of California, San Francisco, CA 94143; [b]Department of Medical Oncology, and Belfer Institute for Applied Cancer Science, Dana-Farber Cancer Institute, Boston, MA 02115; and [c]Department of Pathology, Brigham and Women's Hospital, Harvard Medical School, Boston, MA 02115

Edited* by Inder M. Verma, The Salk Institute for Biological Studies, La Jolla, CA, and approved October 7, 2011 (received for review August 3, 2011)

Preclinical trials in mice represent a critical step in the evaluation of experimental therapeutics. Genetically engineered mouse models (GEMMs) represent a promising platform for the evaluation of drugs, particularly those targeting the tumor microenvironment. We evaluated sunitinib, an angiogenesis inhibitor that targets VEGF and PDGF receptor signaling, in two GEMMs of pancreatic cancer. Sunitinib did not reduce tumor burden in pancreatic ductal adenocarcinoma (PDAC), whereas tumor burden was reduced in the pancreatic neuroendocrine tumor (PNET) model, the latter results confirming and extending previous studies. To explore the basis for the lack of pathologic response in PDAC, we used noninvasive microbubble contrast-enhanced ultrasound imaging, which revealed that sunitinib reduced blood flow both in PDAC and in PNET, concomitant with a reduction in vessel density; nevertheless, PDAC tumors continued to grow, whereas PNET were growth impaired. These results parallel the response in humans, where sunitinib recently garnered FDA and European approval in PNET, whereas two antiangiogenic drugs failed to demonstrate efficacy in PDAC clinical trials. The demonstration of on-target activity but with discordant benefit in the PDAC and PNET GEMMs illustrates the potential value of linked preclinical and clinical trials.

tumor vasculature | experimental cancer therapeutics

Preclinical trials of anticancer drugs in mice are an important step in the drug development process. However, many drugs that are successful in preclinical trials fail in the clinic (1). Genetically engineered mouse models (GEMMs) represent an additional platform that may inform success or failure in humans (2–5). Although tumors in GEMMs may not reflect the full spectrum of heterogeneity and diversity seen in human tumors, they are likely to be well suited to evaluate drugs that target the tumor microenvironment, because critical signaling axes between cancer cells and stroma are not skewed by interspecies differences.

In most cases, GEMMs develop tumors in tissues not amenable to caliper-based monitoring of tumor growth; therefore, as in humans, imaging modalities are desirable to monitor tumor size. Advances in noninvasive imaging both enable such monitoring and allow additional biological questions to be interrogated, such as the functional effect or target modulation of a given drug (6). One evolving technology involves ultrasound imaging, whose sensitivity and content have been improved with microbubbles, a recently developed contrast-enhancing agent. Small, lipid-coated, gas-filled spheres are inoculated into the circulation while recording a two-dimensional ultrasound image. When microbubbles enter the ultrasound field, the vasculature is illuminated owing to the strong reflective properties of microbubbles in the acoustic field. Contrast-enhanced ultrasound is being used increasingly in the clinic (7, 8) and this approach is well suited to monitor the functional effect of angiogenesis inhibitors in GEMMs.

Human pancreatic ductal adenocarcinoma (PDAC) is characterized by stereotypical mutations in oncogenes and tumor suppressor genes: activating mutations in *KRAS*, loss of function mutations in $p16^{INK4a}$, and point mutations in *p53* occur in approximately 95%, 90%, and 75% of tumors, respectively (9). Despite our knowledge of the genetic events contributing to PDAC formation, researchers have been unable to translate this knowledge into effective therapies. The two current standards of care, gemcitabine and erlotinib, each afford only a few weeks of additional survival (10). In addition, FOLFIRINOX (5-fluorouracil, leucovorin, irinotecan, and oxaliplatin) was recently reported to significantly increase survival of patients with pancreatic cancer (11). Seeking to learn more about mechanisms of PDAC, a series of GEMMs have been developed that recapitulate many features of the human cancer (12–16). A distinguishing feature of human PDAC, present as well in the GEMMs, is an abundant desmoplastic stroma (17). This term describes the nonepithelial compartment comprised of large swaths of activated fibroblasts, various immune cell types, and copious amounts of extracellular matrix components produced by the fibroblasts. Embedded within the desmoplasia is a vasculature that is sparse, exhibits poor functionality and is physically separated from the epithelia (18).

We sought in this study to compare and contrast the utility of antiangiogenic therapy in two distinct forms of pancreatic cancer arising de novo in GEMMs. With the vasculature being so sparse in PDAC, we reasoned tumor growth might be critically dependent on what little vasculature exists. Sunitinib is a multityrosine kinase inhibitor that inhibits VEGF receptors (VEGFR), PDGF receptors (PDGFR), and c-Kit at nanomolar concentrations. By targeting VEGFR on tumor endothelial cells, sunitinib should disrupt angiogenesis, whereas its inhibition of PDGFR is expected to impair the function of pericytes, a vascular support cell type (19), as well as the activated cancer-associated fibroblasts that are modulated by PDGF (20, 21). We also employed a GEMM of pancreatic neuroendocrine tumors (PNET), the RIP1-Tag2 model, which has been used extensively for preclinical therapeutic trials (22–26). The preclinical trials reveal divergent responses, with tumor shrinkage in PNET and a lack of objective response in PDAC, congruent with emerging clinical data in both indications.

Author contributions: P.O., G.C.C., O.N.-S., and D.H. designed research; P.O., S.R.P., and O.N.-S. performed research; P.O. contributed new reagents/analytic tools; P.O., G.C.C., O.N.-S., and D.H. analyzed data; and P.O., G.C.C., and D.H. wrote the paper.

Conflict of interest statement: P.O. is currently employed at Pfizer and D.H. is a member of a Pfizer scientific advisory panel.

*This Direct Submission article had a prearranged editor.

Freely available online through the PNAS open access option.

[1]To whom correspondence should be addressed. E-mail: dh@epfl.ch.

[2]Present address: Swiss Institute for Experimental Cancer Research, Swiss Federal Institute of Technology Lausanne, Lausanne, CH-1015, Switzerland.

See Author Summary on page 19455.

This article contains supporting information online at www.pnas.org/lookup/suppl/doi:10.1073/pnas.1111079108/-/DCSupplemental.

Results

Sunitinib Reduces Tumor Burden in GEMMs of PNET but Not PDAC. We sought to compare the effects of angiogenesis inhibition in mouse models of PNET and PDAC. We used two PDAC GEMM models: *Ptf1a-Cre lox-stop-lox(LSL)-Kras^{G12D} p53$^{lox/+}$* mice (13), in which Cre recombinase concomitantly activates the *Kras^{G12D}* oncogene and functionally deletes one allele of the *p53* tumor suppressor in the pancreas; and the *p53* point mutant *Ptf1a-Cre LSL-Kras^{G12D} p53$^{R172H/+}$* (15). The second WT allele of *p53* for both GEMMs is lost during subsequent PDAC tumorigenesis. These tumors present with a prominent desmoplastic component, consisting of α smooth muscle actin (SMA) and PDGFR-ß positive stromal cells (Fig. 1 *A* and *C*). Vascularity of PDAC tumors is sparse. Furthermore, GEMM PDAC tumors show an additional vascular-perfusion mismatch, whereby the tumor vasculature, as judged by endothelial markers CD31 and CD34, exhibits poor functionality by tomato lectin lycopersicon esculentum perfusion studies (Fig. 1 *A* and *B*). By comparison, CD34 and FITC-lectin positive vessels in the duodenum exhibit near complete overlap (Fig. 1*B*, *iii* and *iv*). These stromal and vascular features of the GEMMs parallel those seen in human PDAC (Fig. 1 *C* and *D*).

In the RIP1-Tag2 (RT2) model of PNET, we have previously reported a significant reduction in tumor burden following 5 wk of sunitinib treatment at 40 mg/kg per day (Fig. 2*A*, reprinted from ref. 25 with permission). For our initial comparative evaluation, we examined treatment effects of sunitinib on the *Ptf1a-Cre LSL-Kras^{G12D} p53$^{lox/+}$* mice, as this model exhibits similar synchronicity of tumor development and progression to the PNET model. However, in marked contrast to the PNET model, 4 wk of sunitinib treatment of tumor-bearing *Ptf1a-Cre LSL-Kras^{G12D} p53$^{lox/+}$* mice at 40 mg/kg per day elicited no reduction in tumor burden compared to vehicle-treated animals (Fig. 2*B*).

We then asked whether the combination of gemcitabine and sunitinib would lead to an enhanced response compared to single agent gemcitabine in the PDAC model, because gemcitabine was until recently the standard of care for PDAC patients (27). For this evaluation, *Ptf1a-Cre LSL-Kras^{G12D} p53$^{lox/+}$* mice were given sunitinib at 40 mg/kg per day for 4 wk beginning at 9.5 wk, and then gemcitabine was layered on at 150 mg/kg twice a week for 3 wk beginning at 10.5 wk. At 10.5 wk of age, nearly all mice have developed small tumors that progress on average to end stage between 13 and 16 wk. We initiated sunitinib treatment a week before gemcitabine to allow for potential "vessel normalization" and improved drug delivery, as has been suggested in the application of antiangiogenic therapy (28). This regimen produced a similar response to that observed with gemcitabine alone (Fig. 2 *B* and *C*). Over the course of these trials, between 20% and 30% of control mice succumbed to disease. Whereas gemcitabine as a monotherapy modestly improved survival during the trial, the combination of gemcitabine plus sunitinib had no added benefit, and sunitinib alone showed no efficacy (Fig. 2 *D* and *E*). We also administered gemcitabine at 75 mg/kg twice weekly, but this treatment regimen had no discernible effect (Fig. 2*C*), consistent with the results of a recent study that used either 50 or 100 mg/kg twice a week (18). Hence, sunitinib had no impact on tumor burden in a PDAC GEMM, either as a monotherapy or in combination with gemcitabine.

Microbubble Contrast-Enhanced Ultrasound Can Document Blood Flow in PNET and PDAC Tumors. To noninvasively investigate an anticipated impact of sunitinib treatment in disrupting the functionality of the tumor vasculature, we employed microbubble (mb) contrast-enhanced ultrasound to determine whether intratumoral blood flow was being altered during the course of therapy. This noninvasive imaging technology enables longitudinal assessment of functional blood flow before and after treatment. We first sought to determine how well the microbubble data would compare in different 2D planes of analysis from the same tumor. Because we would not be acquiring data from the same precise plane in serial imaging sessions, we sought to ensure that a two-dimensional measurement would be representative of perfusion across the entire tumor. We therefore acquired microbubble perfusion data from one plane, waited 15 min to allow microbubbles to be removed from the circulation (6), then injected microbubbles again while imaging a different plane at least 2-mm away or perpendicular to the original plane. The data were very similar between the two injections in both PNET and PDAC tumors (Fig. 3), indicating that blood perfusion in these models is relatively homogenous. Notably, for these experiments we employed a second PDAC GEMM, namely, *Ptf1a-Cre LSL-Kras^{G12D} p53$^{R172H/+}$* PDAC mice incorporating the R172H point mutant of the *P53* tumor suppressor (instead of the *Cre*-mediated *p53* gene knockout), because tumors in this model develop more focally and hence are better suited than the multifocal *Ptf1a-Cre LSL-Kras^{G12D} p53$^{lox/+}$* PDAC model for ultrasound-based studies of individual tumors. The concordance and reproducibility of the

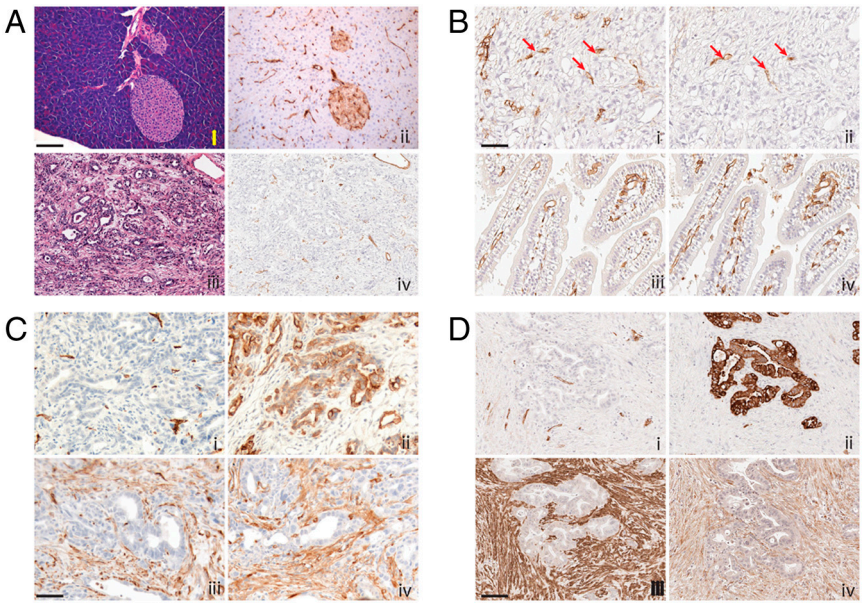

Fig. 1. PDAC arising in *Ptf1a-Cre LSL-Kras^{G12D} p53$^{R172H/+}$* mice have abundant stroma and sparse vasculature. (*A*) Normal mouse pancreas (*i*, *ii*) and PDAC (*iii*, *iv*) stained with H&E (*i*, *iii*) and anti-FITC tomato lectin (*ii*, *iv*). Perfused FITC tomato lectin identifies functional vasculature during physiologic conditions of assay. (*B*) Comparison of total vasculature (anti-CD34; *i*, *iii*) to functionally perfused vasculature (anti-FITC lectin; *ii*, *iv*) within PDAC (*i*, *ii*) and duodenum (*iii*, *iv*) of a single mouse. Red arrows highlight infrequent CD34+ and anti-FITC lectin positive vessels in adjacent sections of PDAC; in the normal tissue, the two are largely concordant. (*C* and *D*) Mouse (*C*) and human (*D*) PDAC stained with (*i*) CD34+ for blood vessels, (*ii*) cytokeratin to highlight tumor cells, (*iii*) α-SMA to identify activated myofibroblasts, and (*iv*) PDGFR-beta. (Magnification: *A*–*C*, 50 μm; *D*. 100 μm.) The lectin perfusion experiment was performed on four untreated mice. All other analyses (CD34, α-SMA, PDGFR-beta, and cytokeratin) were performed on seven untreated or vehicle-treated mice (five vehicle, two no treatment). The selected photomicrographs of invasive tumors immunostained for various antigens are representative of multiple sections of such tumors. Staining pattern among mice within each group showed similar patterns.

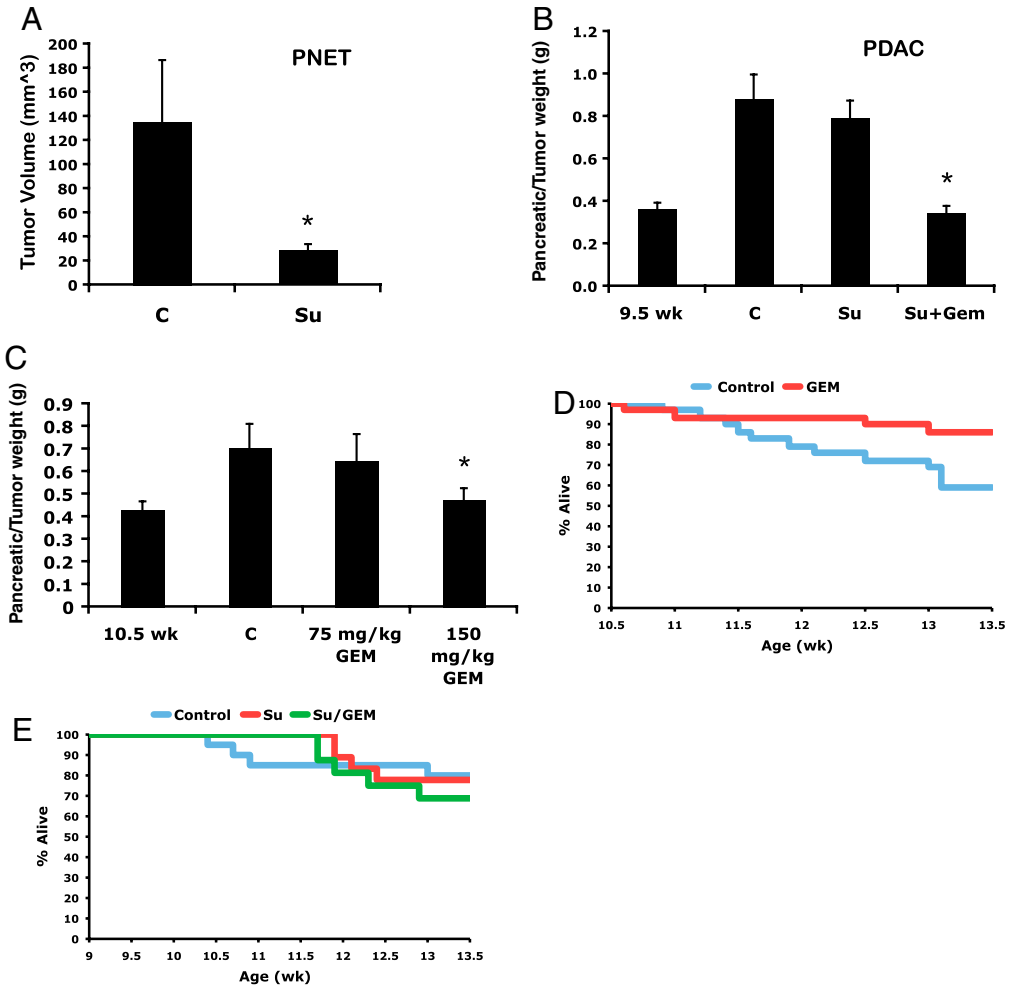

Fig. 2. Effects of sunitinib and gemcitabine in mouse models of PNET and PDAC. (*A*) In PNET, sunitinib caused a reduction in tumor burden following 5 wk of sunitinib treatment. (*B*) Sunitinib showed no efficacy following 4 wk of treatment in *Ptf1a-Cre LSL-Kras^{G12D} p53$^{lox/+}$* mice. The combination of sunitinib plus gemcitabine produced no added benefit to that of gemcitabine alone. (*C*) Gemcitabine at 150 mg/kg twice a week elicited a statistically significant decrease in tumor burden. (*D*) Gemcitabine at 150 mg/kg twice a week affords a survival benefit over the course of the trial. (*E*) Sunitnib or gemcitabine plus sunitinib had no affect on survival during the trial. Bars, SE; *$P < 0.05$; C, vehicle-treated control; Su, sunitinib; Gem, gemcitabine.

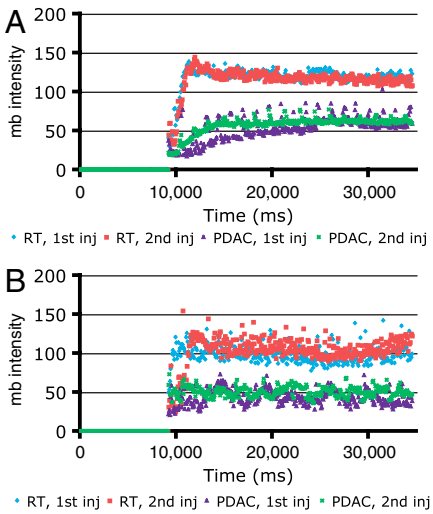

Fig. 3. Independent replicate experiments shown in *A* and *B* evaluating tumor blood flow by microbubble-enhanced ultrasound. Microbubble perfusion data are very similar in different planes of PNET and PDAC tumors, shown in both replicate experiments (*A* and *B*). In both *A* and *B*, red and blue are consecutive injections in different planes of a PNET tumor, whereas green and purple are consecutive injections in different planes of a PDAC tumor. The increase in signal around 10,000 ms is when microbubbles enter the field. After a short "wash-in" period, a plateau is achieved. Note the lower plateau in the PDAC tumors, indicative of comparatively less blood flow despite the fact that these tumors are larger, which further exemplifies the low vascularity of treatment-naïve PDAC tumors.

ultrasound data in both PNET and PDAC encouraged the applicability of contrast-enhanced ultrasound technology to assess the functional vasculature in both forms of pancreatic cancer in the course of sunitinib therapy.

Microbubble Contrast-Enhanced Ultrasound Imaging Demonstrates Reduced Blood Flow in Sunitinib-Treated PNET. Because the RT2 mice develop multifocal PNET disease, 11 to 14-wk-old mice were imaged to identify mice harboring tumors whose location in the pancreas allowed them to be tracked in a subsequent imaging session. All mice selected as having ultrasound-imageable pancreatic tumors were injected with microbubbles to assess the vascularity of tumors before treatment. Cohorts of mice with PNET were then given sunitinib at 40 mg/kg per day or vehicle for 7 or 12 d. On the last day of treatment, mice were again subjected to microbubble contrast-enhanced ultrasound imaging for posttrial assessment. Following 7 or 12 d of sunitinib treatment, all PNET tumors displayed a reduction in microbubble perfusion, reflecting a reduction in the functional vasculature, whereas vehicle-treated tumors exhibited nearly overlapping profiles (Fig. 4 and Movies S1 and S2). This result is in agreement with previous immunohistochemical data showing blood vessel density in PNET is reduced following treatment with sunitinib (25). We also monitored tumor size in response to vehicle or sunitinib treatment and observed tumor shrinkage or stable disease in 9/10 sunitinib-treated tumors, whereas all but one vehicle-treated tumors continued to grow (Fig. 5).

Microbubble Contrast-Enhanced Ultrasound Imaging Reveals Reduction in Blood Perfusion by Sunitinib in PDAC Tumors. To evaluate

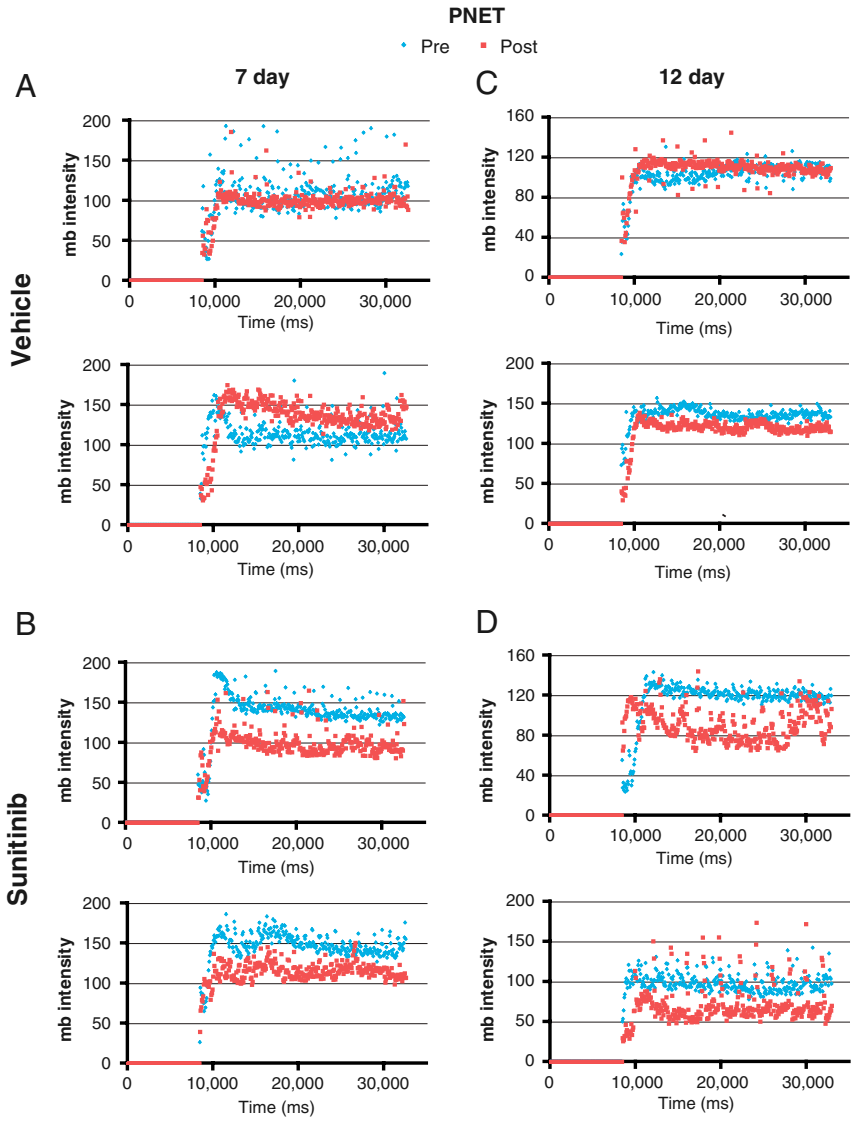

Fig. 4. Sunitinib reduces blood flow in a GEMM of PNET. (*A* and *C*) Vehicle treatment or (*B* and *D*) sunitinib treatment for (*A* and *B*) 7 or (*C* and *D*) 12 d. Blue diamonds, microbubble data acquired before the trial (Pre); red squares, microbubble data acquired at the end of the trial (Post). Comparison of the plateaus of pre- and posttrial microbubble perfusion reveal blood flow is reduced in sunitinib-treated tumors.

PDAC tumors, *Ptf1a-Cre LSL-Kras*^{G12D} *p53*$^{R172H/+}$ mice were imaged by ultrasound every few weeks beginning at 2 mo of age until a tumor was identified (29). Cohorts of mice with similar tumor burden were assembled and treated with sunitinib for 7 or 12 d. Five out of six PDAC tumors in mice treated with sunitinib for 1 wk (Fig. 6) and two out of three tumors from mice treated for 12 d (Fig. 7) displayed a reduction in microbubble perfusion compared to the starting time point when they were imaged and assigned into sunitinib vs control treatment groups (Movies S3 and S4). One tumor from each time point exhibited no change in microbubble perfusion. Interestingly, half of the vehicle-treated tumors also exhibited reduced blood perfusion, suggesting that a subset of PDAC tumors experience a reduction in blood perfusion as part of their natural disease progression. The tumors in the other half of the vehicle-treated cohort exhibited similar microbubble perfusion at both time points. In contrast to the PNET tumor response data, tumor growth was similar irrespective of vehicle or sunitinib treatment in *Ptf1a-Cre LSL-Kras*^{G12D} *p53*$^{R172H/+}$ PDAC tumors (Fig. 8). The average reduction in microbubble perfusion by sunitinib across the cohorts was determined by analyzing the average plateau value (see *Materials and Methods*). In both models, sunitinib-treated tumors showed a similar reduction in perfusion compared to vehicle-treated tumors (Fig. 9). These data confirm sunitinib treatment is not effective in reducing growth of *Kras*, *p53* mutant-driven PDAC tumors, despite markedly disrupting blood flow through the tumor vasculature.

Mean Vessel Density is Significantly Reduced in Sunitinib-Treated PDAC Tumors. Although the reduced blood flow indicated an impact of sunitinib on the functionality of the tumor vasculature, the lack of effect on tumor growth raised questions about the nature and extent of its predicted disruption of vascular morphology in the tumors. Aiming to clarify its effects, tumor-bearing pancreases were sectioned and evaluated by H&E staining and immunohistochemistry. All specimens, regardless of treatment, showed regional histologic topology, involving variable amounts of nontumorous pancreas tissue, viable tumor, and regions of tumor necrosis. To examine tumor vascularity, sections were stained with the endothelial marker CD31 and viable tumor areas were selected for morphologic quantification of vessel density. Sunitinib treatment resulted in a striking reduction in the number of blood vessels in six out of seven PDAC tumors compared to vehicle tumors (Fig. 10 *A* and *B*). To confirm that sunitinib was not selectively reducing the CD31 marker levels beyond visible threshold, adjacent sections were additionally stained with the highly sensitive endothelial marker CD34. Quantification of CD34 showed concordant results (Fig. 10 *A* and *B*). The single sunitinib-treated tumor with blood vessel density similar to that

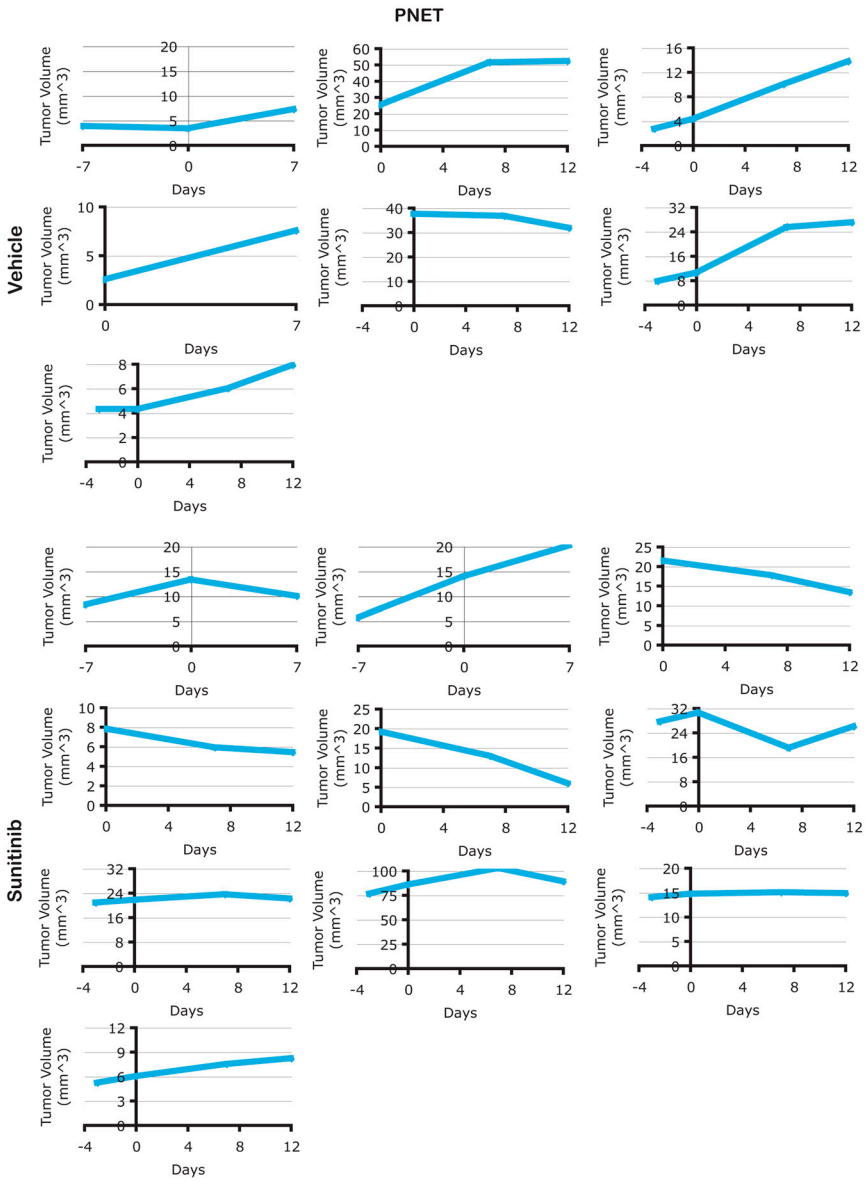

Fig. 5. Individual tumor growth data for vehicle- or sunitinib-treated PNET tumors. Treatment was initiated on day zero. Each panel shows a time-course analysis of an individual PNET tumor. Of note, PNET mice develop multifocal disease and therefore, one to two tumors were tracked for tumor growth in each mouse.

of vehicle-treated tumors bore a different histological appearance, which was further characterized by immunohistochemistry. Unlike the majority of treated and untreated tumors, which showed high levels of cytokeratins and low levels of vimentin, this tumor showed an intermediate phenotype, exhibiting moderate positivity in both cytokeratins and vimentin (Fig. 11) and possibly represents a quasi-mesenchymal PDAC tumor subtype that was recently identified through gene expression profiling (30).

Given sunitinib's targeting of PDGFR signaling, we also assessed PDGFR-ß expression by immunostaining and found it be strongly reduced in the stroma of sunitinib-treated tumors compared to controls. As inhibition of receptor signaling is known to reduce the abundance of PDGFR-β positive cancer associated fibroblasts (CAFs) in other contexts (31), we infer efficacious drug delivery into stromal regions (Fig. 10*A*). Interestingly, although there was a clear reduction in PDGFR-β positive CAFs, we did not detect a reduction in the total stromal content of sunitinib-treated tumors as determined by vimentin staining (Fig 11).

Collectively, these perfusion and histologic data establish that sunitinib was eliciting the expected antiangiogenic effect, but that this loss of vascularity had no impact on tumor burden. The result is striking in that PDAC tumors are already hypovascular and yet appear able to thrive following further vascular reduction.

Discussion

Using standard tumor progression metrics as well as an advanced noninvasive imaging technology, we found that the angiogenesis inhibitor sunitinib elicited striking efficacy in a GEMM of PNET, although the same compound was ineffective in PDAC. As these data mirror results emerging from human trials, this study serves as an example of success and failure in different indications within the same organ of an anticancer drug in clinical practice (32, 33) and in continuing evaluation of possible new indications. In addition, this approach exemplifies how noninvasive imaging methods can be employed to augment the monitoring of drug efficacy.

Pancreatic ductal adenocarcinoma constitutes a cancer type in desperate need of better therapies. The recently developed PDAC GEMMs are poised for pre/coclinical evaluation of candidate drugs, with the potential to help expedite the identifi-

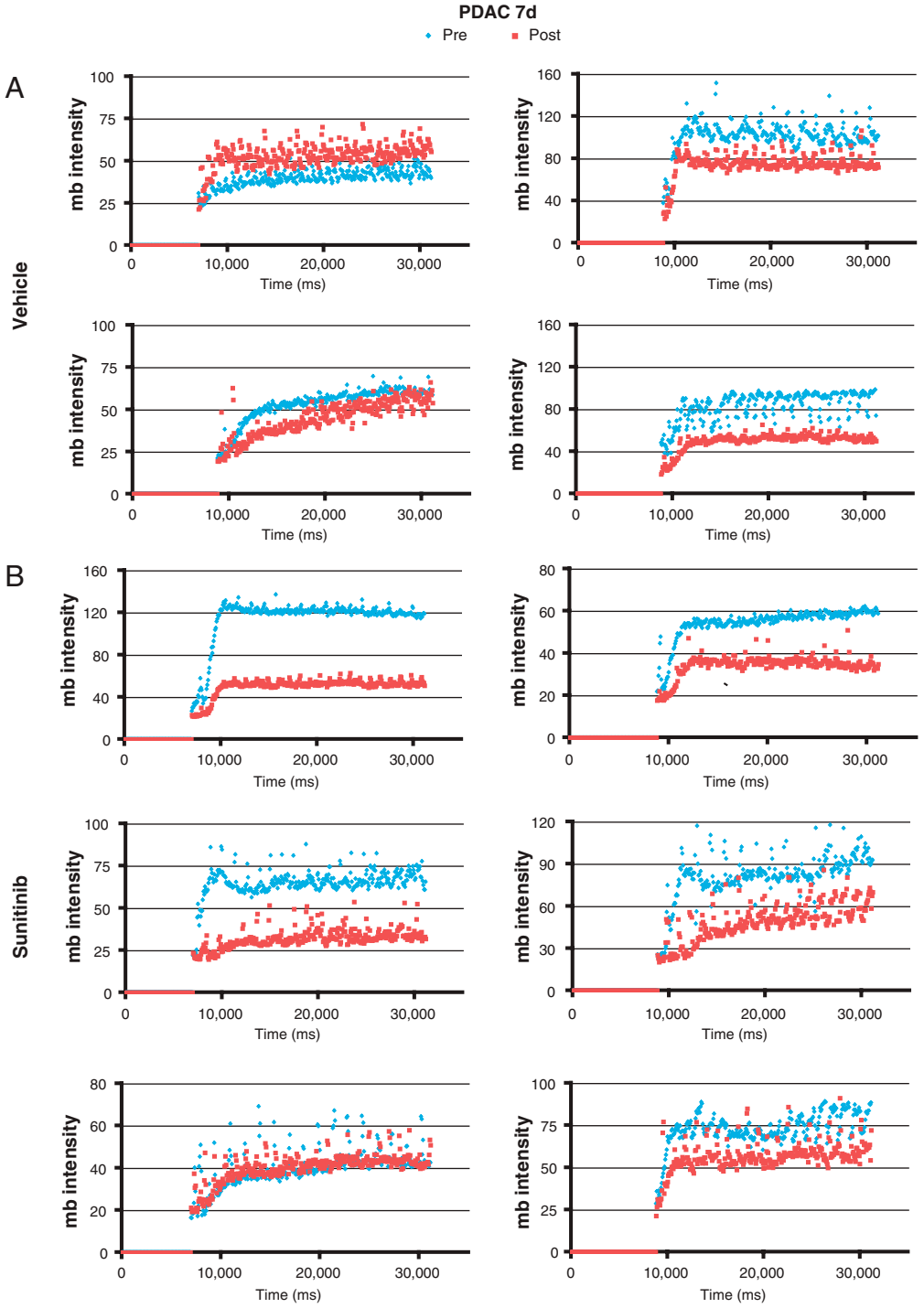

Fig. 6. Microbubble perfusion is reduced in 5/6 tumors from *Ptf1a-Cre LSL-Kras^{G12D} p53$^{R172H/+}$* mice treated with sunitinib for 7 d. (*A*) Microbubble perfusion in vehicle-treated tumors. (*B*) Microbubble perfusion in sunitinib-treated tumors. Note microbubble perfusion is also reduced in half of the vehicle-treated tumors during the 7-d time course. Blue diamonds, microbubble data acquired before the trial (Pre); red squares, microbubble data acquired at the end of the trial (Post).

cation of efficacious therapies. Inhibiting angiogenesis and the desmoplastic tumor microenvironment represented a reasonable hypothesis in the search for new therapies for PDAC. The failure of sunitnib in this stringent in vivo setting argues, however, that angiogenesis inhibitors may not be a tractable therapeutic approach, either alone or in combination with gemcitabine. It should be noted, however, that each angiogenesis inhibitor possesses unique pharmacology and thus it remains formally possible that another angiogenesis inhibitor could prove efficacious. Our data documenting on-target disruption and reduction of the PDAC tumor vasculature with one potent angiogenesis inhibitor suggest that an alternative angiogenesis inhibitor capable of eliciting antitumoral efficacy may well need to have phenotypic effects above and beyond inhibiting tumor angiogenesis.

A recent study using doses of 50 and 100 mg/kg twice weekly (18) found that gemcitabine had little or no effect in *Pdx-1-Cre LSL-Kras^{G12D} p53$^{R172H/+}$* tumors, similar to a dosing regimen where we also observed no efficacy. Thus, in our study, gemcitabine at 75 mg/kg twice weekly also had no effect. We selected our dosing based on previous studies in which 50 mg/kg twice weekly elicited no effect in xenograft studies, whereas 150 mg/kg twice weekly was effective (34, 35).

One explanation for the modest effect of gemcitabine in the clinic involves the demonstration that gemcitabine fails to accumulate in PDAC GEMM tumors that possess an abundant stro-

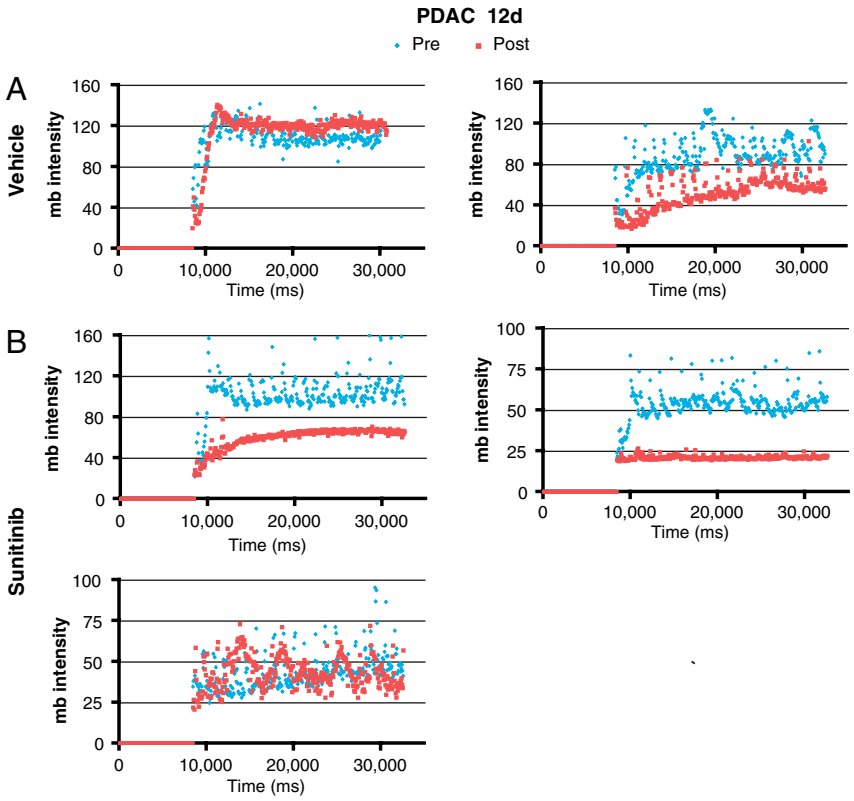

Fig. 7. Microbubble perfusion is reduced in two of three sunitinib-treated and one of two vehicle-treated PDAC tumors from *Ptf1a-Cre LSL-Kras^{G12D} p53$^{R172H/+}$* mice, treated for 12 d. (*A*) Microbubble perfusion in vehicle-treated tumors. (*B*) Microbubble perfusion in sunitinib-treated tumors. Blue diamonds, microbubble data acquired before the trial (Pre); red squares, microbubble data acquired at the end of the trial (Post). Again, one of two untreated controls showed reductions in blood flow over the 12-d period of continuing tumor growth and progression.

mal compartment similar to human tumors. The combination of gemcitabine with an inhibitor of the hedgehog signaling pathway increased perfusion as well as drug efficacy (18). Based on these findings, one might predict the combination of an angiogenesis inhibitor and gemcitabine would diminish any beneficial effect of gemcitabine. We observed a similar decrease in tumor burden between gemcitabine treated and sunitinib plus gemcitabine treated mice. However, there was a modest survival improvement with gemcitabine monotherapy, whereas there was no survival benefit with gemcitabine plus sunitinib. It should be noted that pancreatic tumor burden in the study was assessed indirectly by measuring the weight of the pancreases in mice that survived for the duration of the trial. Whether or not sunitinib treatment actually decreased gemcitabine delivery and whether this in turn blunted a survival advantage afforded by gemcitabine alone requires additional studies.

This study demonstrates the utility of microbubble contrast-enhanced ultrasound as a method to noninvasively monitor the functional effect of an antiangiogenic agent. This imaging modality was in fact able to measure a reduction in blood perfusion following sunitinib therapy in both GEMMs. The reduced mean vessel density as well as the strong reduction in the number of PDGFR-β positive cells in sunitinib-treated tumors confirmed that the drug elicited the expected biological effect on cells expressing its targets, and the microbubbles in addition revealed striking properties of PDAC tumors. First, reduced blood perfusion appears to be a component of disease progression in at least a fraction of PDAC tumors. It is unclear whether this reduced perfusion corresponds to tumors that have developed beyond a certain size or progressed to a distinctive stage of malignancy. The basis for this increasing hypovascularity is unknown but was less dramatic than the reduction observed with sunitinib treatment. Second, although it has been appreciated for some time that PDAC tumors are poorly vascularized, their ability to continue to progress following further therapeutic reduction in vascular density and functionality underscores their apparently limited dependence on the hallmark capability of angiogenesis. It remains a mystery how the tumor epithelia maintains sufficient levels of oxygen and nutrients in such a microenvironment.

Carefully documented failures in preclinical trials could prove as valuable as objective responses, if indeed the failures are factored into decisions on whether to run clinical trials with particular drugs in a given tumor indication. Recent work from our lab demonstrated rapamycin was efficacious in the PNET GEMM used in this study, which mirrored the effect of a "rapalog" in the clinical setting (36). Also, in agreement with our data, a recent study reported that treatment of another PDAC GEMM (involving Kras activation and Ink4A/Arf loss) with gemcitabine plus a VEGF inhibitory antibody did not produce a survival benefit (37). The failures of two VEGF pathway inhibitors, bevacizumab and axitinib, in PDAC clinical trials are concordant with our observed failure of a third, sunitinib, in the PDAC preclinical trial presented in this report. Collectively, the results suggest reconsideration of future clinical trials of other VEGF pathway inhibitors in PDAC unless said drugs are first shown, despite the predictions of these preclinical and clinical trials, to be efficacious in a PDAC GEMM. An additional line of investigation could involve evaluation of orthotopic transplant tumors derived from a panel of cell lines that captures the molecular heterogeneity of human tumors which is not present in the GEMMs (38), to ascertain whether a subset might show tangible benefit and thus become candidates for clinical trials in a preselected population. It is of further interest to note that the aforementioned use of a Hedgehog pathway inhibitor disrupted the desmoplastic stroma and stimulated endothelial cell proliferation in the *Pdx-1-Cre LSL-Kras^{G12D} p53$^{R172H/+}$* model (18), leaving open the possibility that, within the right therapeutic cocktail, angiogenesis inhibitors may yet prove of value in PDAC. In contradistinction, the ability of sunitinib to reduce blood flow and tumor size in a GEMM of PNET is consistent with its efficacy in clinical trials (39, 40), again demonstrating a concordance in outcome between a human cancer and a genetically engineered mouse model thereof. Both the success and the failure of preclinical trials hold promise to guide and prioritize clinical trials, potentially rendering the drug develop-

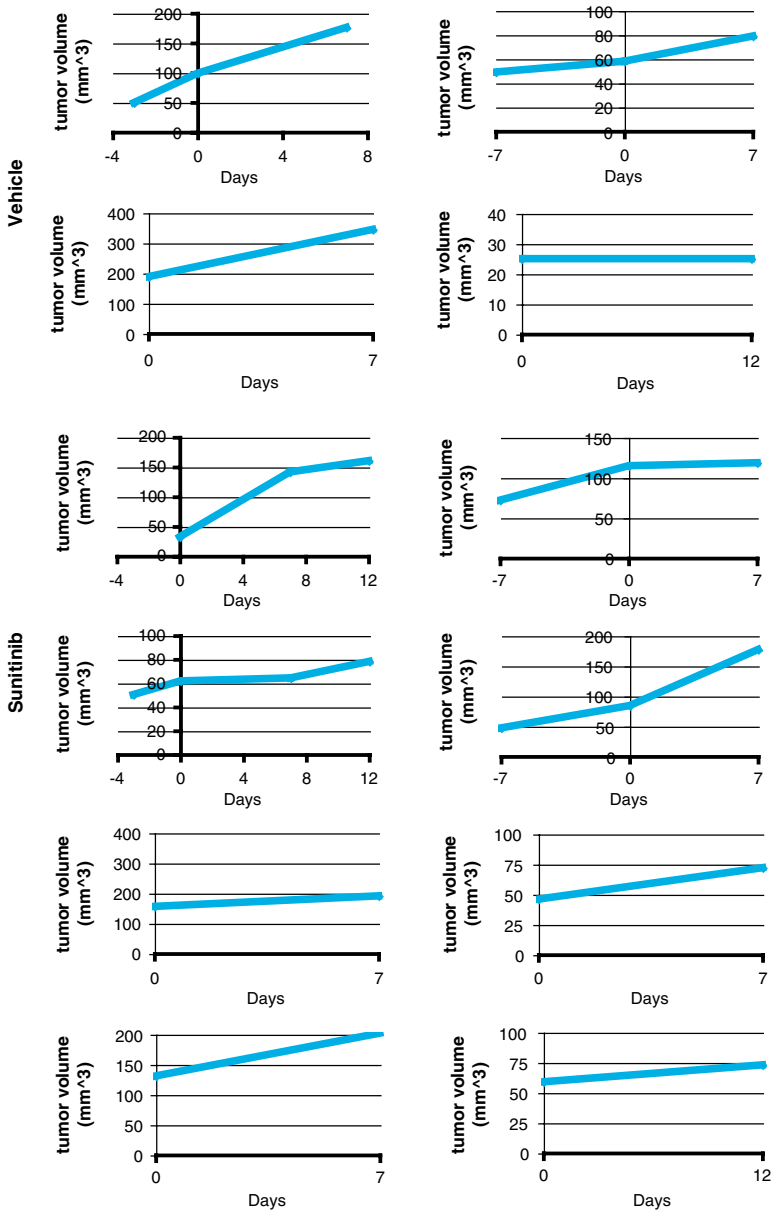

Fig. 8. Individual tumor growth data for vehicle- or sunitinib-treated PDAC tumors. Treatment was initiated on day zero. Each panel shows a time-course analysis of an individual PNET tumor in an independent mouse. The top four graphs represent vehicle-treated tumors.

ment process more efficient and effective in bringing beneficial drugs quickly into practice.

Materials and Methods

Mouse Care and Handling. The generation of RT2 mice has been previously described (24). These animals were on a C57Bl6/CR background. Two versions of the PDAC GEMM were used. Both expressed the activated *Kras*^{G12D} oncogene, but differed in the *p53* tumor suppressor gene mutation that complimented *Kras* in producing PDAC tumors with relative synchronicity in cohorts of age-matched mice. The *p53* floxed PDAC mice harbored the following genetic makeup: *Pft1a-Cre LSL-Kras*^{G12D} *p53*$^{lox/+}$. The *p53* point mutant PDAC mice had the following genetic makeup: *Pft1a-Cre LSL-Kras*^{G12D} *p53*$^{R172H/+}$. Note that, in both models, the wild-type *p53* allele is lost en route to tumor formation. All animal research was performed under the auspices of animal protocols approved by the University of California, San Francisco institutional animal care and use committee.

Immunohistochemistry (IHC) and Immunofluorescence. Normal and tumor mouse tissue were fixed in 10% neutral buffered formalin for 24 h and then processed and embedded in paraffin according to standard protocols. H&E

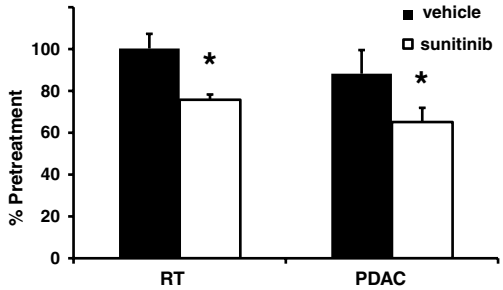

Fig. 9. Microbubble perfusion is reduced by sunitinib treatment to a similar extent in the PNET and PDAC models. Average plateau mb intensity was determined by averaging all values between 20,000 and 30,000 ms which takes into account approximately the second-half of the sequence. Plateau values posttreatment were divided by the pretreatment and multiplied by 100%. Average value across treatment arms was averaged and standard error determined. RT, RIP1-Tag2; Bars, SE; *$P < 0.05$.

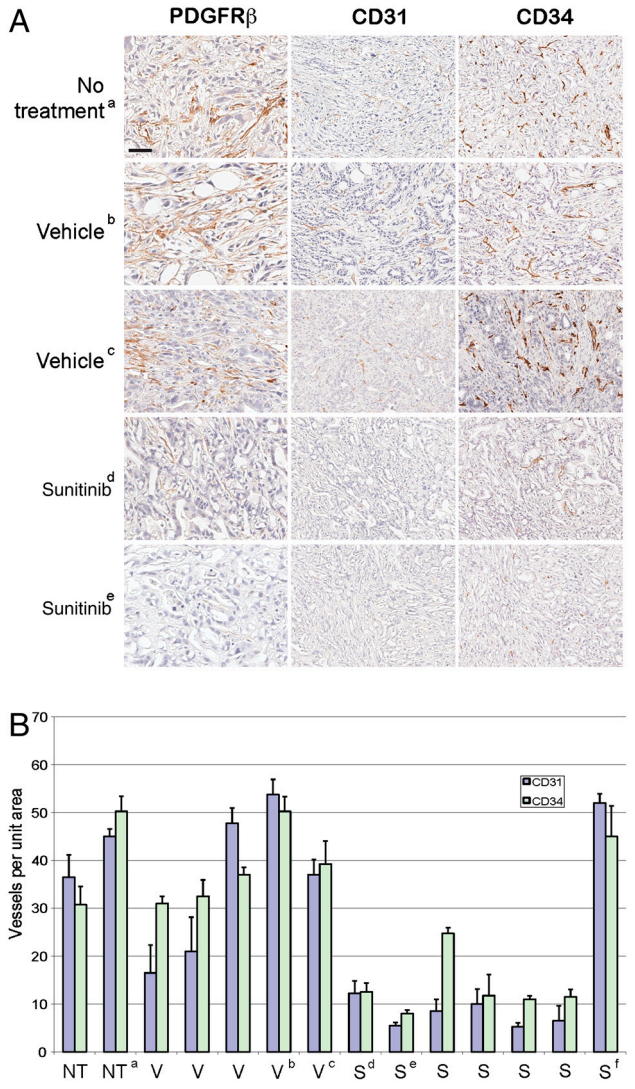

Fig. 10. Vessel density is reduced in PDAC arising in *Ptf1a-Cre LSL-Kras^{G12D} p53$^{R172H/+}$* mice treated with sunitinib. (*A*) Staining of tumors with endothelial markers CD31 and CD34 in control and sunitinib-treated mice to assess microvessel density. Tumors were also stained with PDGFR-beta to evaluate effect of sunitinib treatment on tumor stroma. Magnification bar (shown in the upper left panel) represents 37.5 μm for the PDGFR-beta panel. CD31 and CD34 panels are depicted at twofold lower magnification; a bar of the same length represents 75 μm. All analyses (PDGFR-beta, CD31, and CD34) were performed on seven sunitinib-treated mice and seven controls (five vehicle, two no treatment). The photomicrographs of invasive tumors immunostained for various antigens is representative of staining multiple tissue sections through each tumor. The staining pattern among mice within each group showed similar patterns except for tumor "f" (see Fig. 11). (*B*) CD31 and CD34 positive blood vessels were counted in tumors and averaged over four representative regions and plotted with SEM. Analysis of tumor microvessel density in mice receiving NT, no treatment; V, vehicle; or S, sunitinib.

sections were analyzed first followed by immunohistochemistry. 5-μm fixed sections were incubated with primary antibodies in a hybridization chamber for 1 h at room temperature or overnight at 4 °C. The primary antibodies used were α-SMA (Novus Biologicals), CD34 (MEC14.7, Abcam), CD31 and vimentin (Santa Cruz), PDGFR-beta (C82A3, Cell Signaling), and wide-spectrum screening cytokeratin (Dako). For IHC on human tissue AE1/AE3 (Dako), CD34 (Dako), PDGFR-beta (C82A3, Cell Signaling), α-SMA (1A4, Sigma). Following primary antibody, sections were subsequently incubated for 30 min with goat anti-rabbit IgG(H + L)HRP-conjugated secondary antibody (Dako Envision kit), then visualized with diaminobenzidine (DAB) and counterstained with Mayer's Hematoxylin. To quantify microvessel density, chromatic CD34- and CD31-stained slides were digitally scanned using the Scanscope XT slide scanning platform (Aperio). Four representative regions within an invasive tumor, each 640 × 640 μm were selected for quantification. Vessels in each region were manually counted and charted. For tumors that were treated with drug, animals were euthanized 7 or 12 d after initiation of treatment.

FITC-Lectin Perfusion of Mice. Five minutes prior to euthanasia, mice were anesthetized with 2.5% Avertin (Sigma). Fluorescein lycopersicon esculentum (tomato) lectin (Vector) was diluted 1:1 in water and 100 μL injected retroorbitally. After 5 min, mice were heart perfused with 10 mL PBS, followed by 10 mL Zn-buffered formalin (Medical Chemical Corporation). Tissue were dissected and incubated at 4 °C in formalin for 2–4 h and transferred to 30% sucrose overnight, then frozen in Tissue Tek O.C.T. (optimal cutting temperature). Samples were also paraffin embedded. Ten- and 30-μm sections were cut and analyzed using a fluorescent microscope. As a control, livers were examined and were consistent in FITC-lectin intensity between all animals. For formalin fixed, paraffin embedded samples, IHC was performed (described above) using a rabbit anti-FITC (Invitrogen) primary antibody. Staining of FITC-lectin perfusion was then analyzed using DAB immunohistochemistry.

Experimental Therapeutic Trials. For PNET trials, 9.5-wk-old RT2 mice were given either 40 mg/kg sunitinib or vehicle (0.5% carboxymethylcellulose, 1.8% NaCl, 0.4% Tween 80, 0.9% benzyl alcohol, and reverse osmosis deionized water adjusted to pH 6) alone via oral gavage for 5 wk. Tumor volume was determined as described previously (41). For *Pft1a-Cre LSL-Kras^{G12D} p53$^{lox/+}$* mice, 9.5-wk-old mice were given either 40 mg/kg sunitinib or vehicle via oral gavage for 4 wk. Gemcitabine (Gemzar, Eli Lilly Co.) was administered to 10.5-wk-old mice at 150 or 75 mg/kg injected i.p. twice weekly for 3 wk. For sunitinib plus gemcitabine combination therapy, mice received sunitinib beginning at 9.5 wk and gemcitabine beginning at 10.5 wk. PDAC mice were euthanized and tumor-containing pancreata were dissected and weighed (n = 13–18 per group). For *Pft1a-Cre LSL-Kras^{G12D} p53$^{R172H/+}$* mice, animals were ultrasound imaged and when a tumor was identified the animal was enrolled in trial for 7 or 12 d. Tumor size was determined by 3D determination using the VisualSonics software.

Microbubble Contrast-Enhanced Ultrasound Analysis of Tumors. Ultrasound was performed using a Vevo770 from VisualSonics, Inc., using the 40-MHz 704 probe at 50% transmit power in for microbubble imaging per manufacturer's instructions. Mice were anesthetized using 2% isofluorane at approximately 2 L/min and hair was removed over the abdomen. Body temperature was monitored using a rectal probe and kept within 1° of 37 °C using a heated stage and a heat lamp. Ultrasound gel was used. PDAC mice were imaged approximately twice a month until tumors at least approximately 2–5 mm in diameter were detected. Three-dimensional tumor images were acquired using the 3D acquisition motor and images analyzed using VisualSonics, Inc. imaging software package. For tumor vasculature imaging, one vial of nontargeted microbubbles (VisualSonics, Inc.) was resuspended in 1.2 mL saline. After drawing up 60 μL into a 28-gauge insulin syringe (Becton Dickinson), the needle was inserted into the tail vein. A pretrig cine loop was then initiated to collect the reference and, after approximately 8 s, microbubbles were injected. The cine loop was collected for 550 frames total, which is just less than 1 min. The point at which microbubbbles entered the plane was then determined and the background reference subtracted. Data were averaged over 32 frames and exported. Tumor-bearing mice were injected with microbubbles and then enrolled in therapeutic trials. At the end of treatment, mice were injected with microbubbles again. Tumor plane sizes were similar at both time points.

For microbubble perfusion analysis, contrast was set to 40 and threshold set to zero. The tumor was selected as the contrast region and Reference Subtracted Mean data were used. To align the data, the time point at which signal increased over zero was identified and normalized to the same time point across all tumors. Microbubble plateaus were also normalized such that all datasets were identical in length by adjusting the ends of the plateaus so that all cine loop datasets were the same time length for all injections for an experiment. For comparing the effect of angiogenesis inhibitors across cohorts, average plateau values were determined by averaging mb intensity between 20,000 and 30,000 and determining the percent change between pre- and poststudy. Standard error of the mean and student's t test (one-tailed) were used. To generate 2D images, after acquiring the microbubble perfusion movie, Maximum Intensity Perfusion was selected and processed. This setting generates a 2D image that marks any pixel green if a microbubble passes through that pixel at any point in time over the duration of the movie.

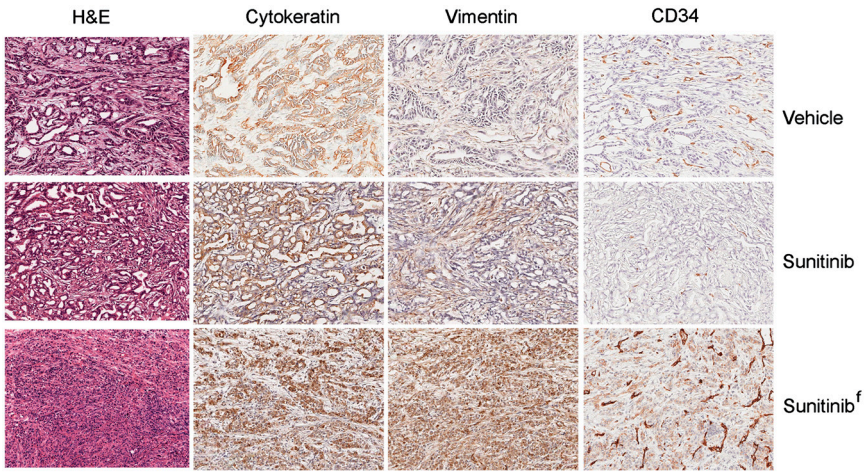

Fig. 11. The sunitinib-treated PDAC tumor showing a lack of vascular attenuation has atypical morphologic features. The upper and middle rows represent typical PDAC tumors treated with vehicle or sunitinib, whereas the lower row shows the atypical tumor (tumor f from Fig. 10) that did not suffer loss of vascularity in response to sunitinib therapy. Typical PDAC tumors stained positive for cytokeratins and negative for vimentin. Tumor f demonstrates positivity for both markers as well as more poorly differentiated morphology. CD34, used to demonstrate vasculature, is also aberrantly expressed on tumor f cells.

ACKNOWLEDGMENTS. We thank James Christensen (Pfizer, Inc.) for providing sunitinib and Dana Hu-Lowe (Pfizer, Inc.) for critical reading of the manuscript. We thank Marina Vayner, Susan Cacacho, Cristina Guinto, and Ehud Drori for excellent technical assistance. Research by P.O., G.C.C., S.R.P., O.N.-S., and D.H. was supported by National Institutes of Health (NIH) 5P01CA117969-04 (Principal Investigator Ronald DePinho); P.O., O.N.-S., and D.H. were supported by Gastrointestinal Specialized Programs of Research Excellence in Gastrointestinal Cancers NIH 1P50CA127003-02 and by The William K. Bowes Jr. Foundation. D.H. is an American Cancer Society Research Professor. P.O. acknowledges salary support from National Cancer Institute Training Grant T32 CA09043 (Director J. Michael Bishop), Molecular Analysis of Tumor Viruses. P.O., O.N.-S., and D.H. acknowledge access to the University of California, San Francisco (UCSF), Diabetes Center's Microscopy Core (funded by Diabetes and Endocrinology Research Center) and to the Preclinical Therapeutic Core at UCSF. G.C.C. and S.R.P recognize histology support provided by the Specialized Histopathology and Rodent Histopathology Cores (Dana-Farber/Harvard Cancer Center).

1. Kola I, Landis J (2004) Can the pharmaceutical industry reduce attrition rates? *Nat Rev Drug Discov* 3:711–715.
2. Carver BS, Pandolfi PP (2006) Mouse modeling in oncologic preclinical and translational research. *Clin Cancer Res* 12:5305–5311.
3. Frese KK, Tuveson DA (2007) Maximizing mouse cancer models. *Nat Rev Cancer* 7:645–658.
4. Sharpless NE, Depinho RA (2006) The mighty mouse: Genetically engineered mouse models in cancer drug development. *Nat Rev Drug Discov* 5:741–754.
5. Tuveson D, Hanahan D (2011) Translational medicine: Cancer lessons from mice to humans. *Nature* 471:316–317.
6. Willmann JK, van Bruggen N, Dinkelborg LM, Gambhir SS (2008) Molecular imaging in drug development. *Nat Rev Drug Discov* 7:591–607.
7. Sakamoto H, et al. (2008) Utility of contrast-enhanced endoscopic ultrasonography for diagnosis of small pancreatic carcinomas. *Ultrasound Med Biol* 34:525–532.
8. Sofuni A, et al. (2005) Differential diagnosis of pancreatic tumors using ultrasound contrast imaging. *J Gastroenterol* 40:518–525.
9. Hruban RH, Iacobuzio-Donahue C, Wilentz RE, Goggins M, Kern SE (2001) Molecular pathology of pancreatic cancer. *Cancer J* 7:251–258.
10. Moore MJ, et al. (2007) Erlotinib plus gemcitabine compared with gemcitabine alone in patients with advanced pancreatic cancer: A phase III trial of the National Cancer Institute of Canada Clinical Trials Group. *J Clin Oncol* 25:1960–1966.
11. Conroy T, et al. (2011) FOLFIRINOX versus gemcitabine for metastatic pancreatic cancer. *N Engl J Med* 364:1817–1825.
12. Aguirre AJ, et al. (2003) Activated Kras and Ink4a/Arf deficiency cooperate to produce metastatic pancreatic ductal adenocarcinoma. *Genes Dev* 17:3112–3126.
13. Bardeesy N, et al. (2006) Both p16(Ink4a) and the p19(Arf)-p53 pathway constrain progression of pancreatic adenocarcinoma in the mouse. *Proc Natl Acad Sci USA* 103:5947–5952.
14. Hingorani SR, et al. (2003) Preinvasive and invasive ductal pancreatic cancer and its early detection in the mouse. *Cancer Cell* 4:437–450.
15. Hingorani SR, et al. (2005) Trp53R172H and KrasG12D cooperate to promote chromosomal instability and widely metastatic pancreatic ductal adenocarcinoma in mice. *Cancer Cell* 7:469–483.
16. Olive KP, et al. (2004) Mutant p53 gain of function in two mouse models of Li-Fraumeni syndrome. *Cell* 119:847–860.
17. Chu GC, Kimmelman AC, Hezel AF, DePinho RA (2007) Stromal biology of pancreatic cancer. *J Cell Biochem* 101:887–907.
18. Olive KP, et al. (2009) Inhibition of Hedgehog signaling enhances delivery of chemotherapy in a mouse model of pancreatic cancer. *Science* 324:1457–1461.
19. Bergers G, Song S, Meyer-Morse N, Bergsland E, Hanahan D (2003) Benefits of targeting both pericytes and endothelial cells in the tumor vasculature with kinase inhibitors. *J Clin Invest* 111:1287–1295.
20. Jaster R (2004) Molecular regulation of pancreatic stellate cell function. *Mol Cancer* 3:26.
21. Jaster R, et al. (2003) Regulation of pancreatic stellate cell function in vitro: Biological and molecular effects of all-trans retinoic acid. *Biochem Pharmacol* 66:633–641.
22. Bergers G, Hanahan D (2002) Combining antiangiogenic agents with metronomic chemotherapy enhances efficacy against late-stage pancreatic islet carcinomas in mice. *Cold Spring Harb Symp Quant Biol* 67:293–300.
23. Casanovas O, Hicklin DJ, Bergers G, Hanahan D (2005) Drug resistance by evasion of antiangiogenic targeting of VEGF signaling in late-stage pancreatic islet tumors. *Cancer Cell* 8:299–309.
24. Hanahan D (1985) Heritable formation of pancreatic beta-cell tumours in transgenic mice expressing recombinant insulin/simian virus 40 oncogenes. *Nature* 315:115–122.
25. Paez-Ribes M, et al. (2009) Antiangiogenic therapy elicits malignant progression of tumors to increased local invasion and distant metastasis. *Cancer Cell* 15:220–231.
26. Pietras K, Hanahan D (2005) A multitargeted, metronomic, and maximum-tolerated dose "hemo-switch" regimen is antiangiogenic, producing objective responses and survival benefit in a mouse model of cancer. *J Clin Oncol* 23:939–952.
27. Burris HA, 3rd, et al. (1997) Improvements in survival and clinical benefit with gemcitabine as first-line therapy for patients with advanced pancreas cancer: A randomized trial. *J Clin Oncol* 15:2403–2413.
28. Jain RK (2001) Normalizing tumor vasculature with anti-angiogenic therapy: A new paradigm for combination therapy. *Nat Med* 7:987–989.
29. Cook N, Olive KP, Frese K, Tuveson DA (2008) K-Ras-driven pancreatic cancer mouse model for anticancer inhibitor analyses. *Methods Enzymol* 439:73–85.
30. Collisson EA, et al. (2011) Subtypes of pancreatic ductal adenocarcinoma and their differing responses to therapy. *Nat Med* 17:500–503.
31. Furuhashi M, et al. (2004) Platelet-derived growth factor production by B16 melanoma cells leads to increased pericyte abundance in tumors and an associated increase in tumor growth rate. *Cancer Res* 64:2725–2733.
32. Kindler HL, et al. (2011) Axitinib plus gemcitabine versus placebo plus gemcitabine in patients with advanced pancreatic adenocarcinoma: A double-blind randomised phase 3 study. *Lancet Oncol* 12:256–262.
33. Kindler HL, et al. (2010) Gemcitabine plus bevacizumab compared with gemcitabine plus placebo in patients with advanced pancreatic cancer: Phase III trial of the Cancer and Leukemia Group B (CALGB 80303). *J Clin Oncol* 28:3617–3622.
34. Amoh Y, et al. (2006) Visualization of nascent tumor angiogenesis in lung and liver metastasis by differential dual-color fluorescence imaging in nestin-linked-GFP mice. *Clin Exp Metastasis* 23:315–322.
35. Yokoi K, et al. (2005) Simultaneous inhibition of EGFR, VEGFR, and platelet-derived growth factor receptor signaling combined with gemcitabine produces therapy of human pancreatic carcinoma and prolongs survival in an orthotopic nude mouse model. *Cancer Res* 65:10371–10380.
36. Chiu CW, Nozawa H, Hanahan D (2010) Survival benefit with proapoptotic molecular and pathologic responses from dual targeting of mammalian target of rapamycin and epidermal growth factor receptor in a preclinical model of pancreatic neuroendocrine carcinogenesis. *J Clin Oncol* 28:4425–4433.
37. Singh M, et al. (2010) Assessing therapeutic responses in Kras mutant cancers using genetically engineered mouse models. *Nat Biotechnol* 28:585–593.
38. Bagri A, et al. (2010) Effects of anti-VEGF treatment duration on tumor growth, tumor regrowth, and treatment efficacy. *Clin Cancer Res* 16:3887–3900.
39. Kulke MH, et al. (2008) Activity of sunitinib in patients with advanced neuroendocrine tumors. *J Clin Oncol* 26:3403–3410.
40. Raymond E, et al. (2011) Sunitinib malate for the treatment of pancreatic neuroendocrine tumors. *N Engl J Med* 364:501–513.
41. Inoue M, Hager JH, Ferrara N, Gerber HP, Hanahan D (2002) VEGF-A has a critical, nonredundant role in angiogenic switching and pancreatic beta cell carcinogenesis. *Cancer Cell* 1:193–202.